Composite Structures 340 (2024) 118135

Contents lists available at ScienceDirect

Composite Structures

journal homepage: www.elsevier.com/locate/compstruct

Compressive properties and energy absorption of 4D printed auxetic mechanical metamaterials

Bingxun Li [a,1], Xiaozhou Xin [a,1], Cheng Lin [b], Liwu Liu [a,*], Yanju Liu [a,*], Jinsong Leng [b]

[a] Department of Astronautical Science and Mechanics, Harbin Institute of Technology (HIT), P.O. Box 301, No. 92 West Dazhi Street, Harbin 150001, People's Republic of China

[b] Center for Composite Materials and Structures, Harbin Institute of Technology (HIT), P.O. Box 3011, No. 2 Yikuang Street, Harbin 150080, People's Republic of China

ARTICLE INFO

Keywords:
4D printing
Shape memory polymer
Auxetic metamaterial
Energy absorption
Programmable and reconfigurable
Quasi-static compression

ABSTRACT

Auxetic mechanical metamaterials contract or expand laterally when subjected to compressive or tensile load in the axial direction and offer potential benefits in areas such as flexible electronics, aerospace, and soft actuators. Nevertheless, when metamaterials are fabricated using conventional methods, their configurations and properties are fixed, which prohibits adaptation to the specific geometric requirements of their application environment. This limits their further development. This paper proposes an auxetic mechanical metamaterial with a negative Poisson's ratio and energy absorption capability. Compression specimens are fabricated with LCD photo-curable printing technology. The deformation mechanism and in-plane compression characteristics are examined through experimental and numerical simulation methods. The influence of unit cell geometrical control parameters on Poisson's ratio and energy absorption are also explored. The results indicate the dominant deformation mechanism of metamaterial during in-plane compression is bending deformation. The negative Poisson's ratio behavior is more pronounced when compressing along the X direction than along the Y direction, and the specimens also exhibit energy absorption capacity. In addition, the metamaterials prepared by 4D printing technology can be transformed from one configuration to another under external stimuli stimulation and force, and exhibit different mechanical properties, realizing programmable and reconfigurable, further expanding their application range.

1. Introduction

Metamaterials are a new type of functional materials composed of artificial microstructure units, and exhibit extraordinary physical properties that are not generally observed in natural materials [1], such as negative refractive index [2], thermal cloak [3], negative thermal expansion [4], negative stiffness [5], lightweight and ultrahigh strength [6,7], tunable phononic wave propagation [8], etc. Mechanical metamaterials refer to a kind of metamaterials with exceptional mechanical characteristics derived from their geometrical structure [1]. These characteristics include negative Poisson's ratio [9–11], zero Poisson's ratio [12], bistability [13], compression-torsion coupled deformation [14,15], energy absorption [16–18], etc. These features make mechanical metamaterials highly distinctive. In the past few decades, numerous studies have been conducted on the mechanical characteristics.

Under axial tensile or compressive load, the auxetic metamaterial expands or contracts perpendicular to the load, exhibiting excellent mechanical performance such as fracture resistance, indentation resistance, negative Poisson's ratio, energy absorption, and more. Since the fabrication of auxetic foams was first reported by Lakes [19] in 1987, researchers have been carried out a lot of research on the design, preparation, and the related performance of auxetic metamaterials [20–22]. Their potential applications have been demonstrated in flexible electronics [23], biomedicine [24,25], soft actuators [26,27] and other fields. The common auxetic structures currently available include re-entrant structures, rotating structures, chiral and anti-chiral structures and buckling deformation-guided structures [28]. To improve the energy absorption, Ren et al. [29] developed a lightweight auxetic metamaterial utilizing elliptical perforated plates. Small deformation regions were removed while large deformation regions were retained to achieve optimization. The metamaterial maintained its mechanical properties while significantly improving its specific energy absorption

* Corresponding authors.
E-mail addresses: liulw@hit.edu.cn (L. Liu), yj_liu@hit.edu.cn (Y. Liu).
[1] These authors contributed equally to this work.

https://doi.org/10.1016/j.compstruct.2024.118135
Received 26 December 2023; Received in revised form 1 March 2024; Accepted 12 April 2024
Available online 22 April 2024

capacity. Zhang et al. [30] put forward a novel Re-S-AC metamaterial, featuring a re-entrant star-shape anti-chiral. They conducted experimental and finite element analyses to explore its deformation mechanism and mechanical properties. Compared to the anti-tetrachiral and re-entrant star-shaped structures, the proposed Re-S-AC had the highest mean compression stress at a given thickness and mass. Liu et al. [31] introduced three star-rhombus honeycombs by incorporating rhombic components into the conventional star honeycomb. Based on the finite element method, they investigated their quasi-static crushing responses. The results demonstrated that introducing rhombic components significantly enlarged specific energy absorption and crushing stress. Additionally, the location and arrangement manner of the rhombic components influenced the Poisson's ratio considerably. Hopkins et al. [32] combined negative Poisson's ratio honeycomb with conventional positive Poisson's ratio honeycomb to design a metamaterial capable of achieving alternating Poisson's ratio. It was obtained through a rational adjustment of the geometric parameters of the contacting bodies, enabling them to move and collide in a particular time series when subjected to compression or tension, achieving the desired alternating Poisson's ratio.

Researchers have also conducted studies on the dynamic mechanical properties of honeycomb structures. Shi et al. [33] developed auxetic metamaterials featuring cell-wall angle gradient, and used dynamic finite element analysis to study their planar impact resistance performance. The results showed that under quasi-static compression or low velocity impact, the angle gradient design provides excellent energy absorption capabilities. Whereas as the impact velocity increased, energy absorption only increased when the gradient was arranged in a particular direction. This discovery offers a novel approach to applying mechanical metamaterials. Furthermore, by integrating a gradient design approach with a fractal self-similarity configuration, Ng et al. [34] proposed a new fractal honeycomb. They studied the effects of various factors, including gradient arrangement, honeycomb wall thickness and impact velocity, on the dynamic stress–strain relationship and honeycomb energy absorbing capacity through finite element models. Compared to the conventional honeycomb, graded fractal honeycomb showed significant improvement in energy absorption capacity and average crushing force.

As previously mentioned, the mechanical performance of mechanical metamaterials depends on their microstructure geometric configuration. When geometric parameters of the metamaterials are established, their mechanical properties become fixed, thereby limiting their further development and application. To overcome this problem, researchers have developed various excitation response materials, such as magnetic drive [35,36], thermal drive [37], and so on. Lv et al. [38] used shape memory material (PLA) to fabricate a novel auxetic metamaterial through 3D printing technology. The printed 2D meshes could be programmed and reconfigured, achieving the continuous programmability of Poisson's ratio, modulus, and fracture strain after fabrication. Leng et al.[39] have proposed 4D printed metamaterials with tunable, programmable, and reconfigurable characteristics. Their stress–strain curves have shown similarity with the "J"-shaped stress–strain curves of biomaterials. The programmability and reconfigurability of metamaterials allowed high precision conversion of mechanical behavior between different biomaterials. Finally, potential applications in tissue engineering and flexible electronics were demonstrated.

In this work, mechanical metamaterials with energy absorption capacity and negative Poisson's ratio were firstly designed by combining 4D printing technology and shape memory materials. Secondly, the compressive deformation mechanism and in-plane mechanical properties along the X and Y directions were characterized, and a parameterized study was carried out. Finally, the programmable and reconfigurable properties of the metamaterials were characterized through a hot water bath. Following programming and reconfiguration, the metamaterials display varying mechanical properties, achieving adjustable configuration and mechanical behavior, thereby expanding their potential applications.

2. Design and fabrication

2.1. Geometric design of unit cell

In this work, metamaterials with negative Poisson's ratio and energy absorption are designed and manufactured. As depicted in Fig. 1(a), the two horizontal beams on the top and bottom of a square with side length L_1 are replaced by two inward-crossing tilted cell walls, while also arranging two vertical beams at their intersection. The two vertically oriented beams on the left and right sides are replaced by two outward-crossing tilted cell walls. At the same time, four horizontal beams are prolonged on the four vertices of the square to obtain unit cell of the auxetic mechanical metamaterials. For the convenience of subsequent analysis, the beams arranged in X and Y direction are called X-direction cell walls and Y-direction cell walls, and the beams crossing inward or outward are termed as the inclined cell walls.

There are eight parameters controlling the geometrical configuration and mechanical characteristics of the metamaterial unit cell, namely L_1 L_2 d_1 d_2 t_1 t_2 s w. Among them,L_1 refers to the distance between the X-direction cell walls, L_2 represents the length of the X-direction cell walls of the unit cell, d_1 is the Y-direction tilt distance of the inward-cross tilted cell walls,d_2 represents the X-direction tilt distance of the outward-cross tilted cell walls, t_1 is the width of the Y-direction cell walls, t_2 refers to the width of all the rest of the cell walls, and s is the vertical distance between the top of the cell walls in the Y direction and the top of the extended X-direction cell walls. It is specified that when $s = 0$,the corresponding situation is to cancel the arrangement of the Y-direction cell walls with a thickness of t_1. w is the out-of-place thickness of metamaterial. In this work, the out-of-plane thickness is $w = 20$ mm.

After arraying the unit cell as shown in Fig. 1(a), stiffening walls are placed both below and above the metamaterial to carry the load. Subsequently, the mechanical characteristics of the metamaterial in various directions are evaluated. Fig. 1(b) illustrates the CAD models during compressing in the X direction and Y direction.

2.2. Specimen manufacturing

This work utilizes a 4D printing technique-LCD photocuring printing to manufacture metamaterials with high precision. Liquid photosensitive resin is used, and it can form Shape Memory Polymers (SMP). Fig. 1 (c) illustrates the working principle of the LCD curing printer, which employs an LCD screen to generate images. When the printer works, the LCD screen displays selective transparent areas, which are then illuminated by ultraviolet light of a particular wavelength and intensity. This process enables the photosensitive liquid resin to be cured and adhere to the build platform. When printing the next layer, the build platform raises the cured portion to allow the liquid resin to reflow. Once the resin has filled the underside of the platform, it drops again. This process is repeated, and the resin between the specimen and the release film is cured by the UV light, layer by layer, to complete the printing. More information about the manufacturing of specimens can be found in the supporting information.

3. Method and model

3.1. Matrix material testing

Dumbbell-shaped standard specimens were manufactured utilizing LCD photocuring printing technology. Material properties were characterized via quasi-static tensile experiments conducted at a constant speed of 2 mm per minute. According to the stress–strain curve of the photosensitive resin obtained from the tensile experiment as illustrated in Fig.S1, the Young's modulus $E = 274$ MPa, the fracture strain $\delta = 75.5\%$ and the strength limit $\sigma_b = 19.10$ kPa.

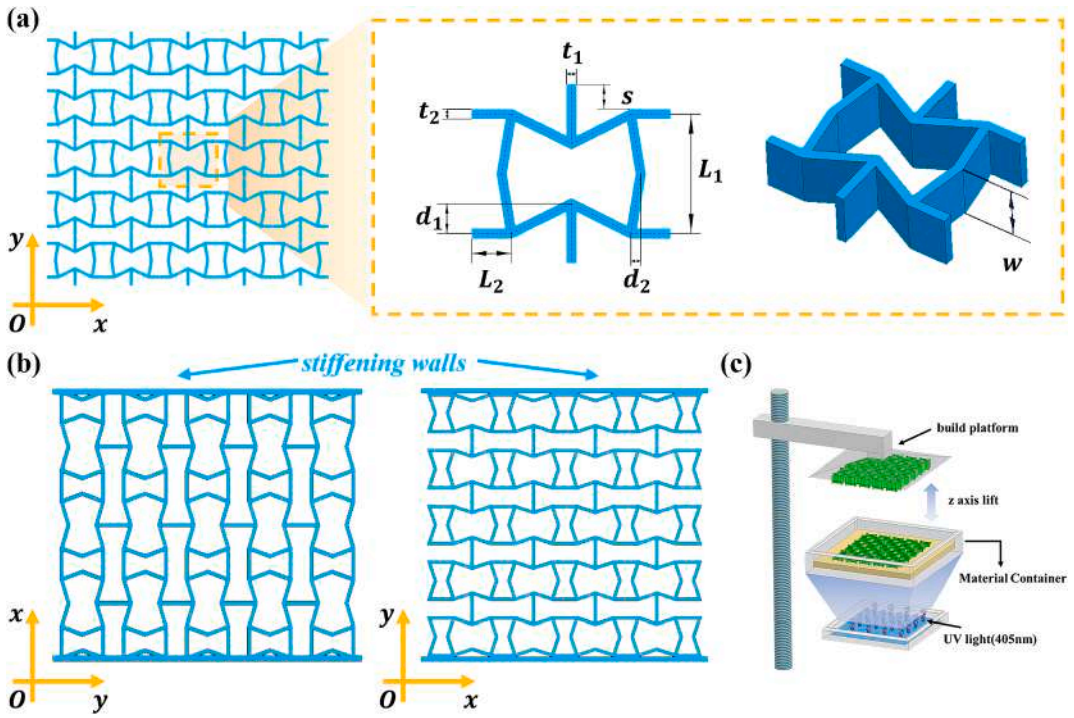

Fig. 1. Design and manufacture of auxetic metamaterials: (a) unit cell and geometrical parameters; (b) CAD models of the metamaterials during compression along the X and Y directions; (c) the manufacturing process of auxetic metamaterials.

3.2. Quasi-static compression testing

The Zwick-010 tensile machine was used to conducted quasi-static compression tests on prepared specimens. The compression testing was carried out at a constant speed of 2 mm per minute, while the compression process was recorded using a Sony IMX766 to capture the deformation of metamaterials.

3.3. Finite element model

ABAQUS/Explicit was used to simulate the compression process, and the material parameters of finite element model were obtained from the tensile experiments of the dumbbell-shaped standard specimens. The model comprised of three components: the upper and lower platens, and mechanics metamaterial positioned in the center. The upper and lower platens were modelled as 3D analytical rigid bodies with reference points, whilst the auxetic mechanical metamaterial was modeled as a 3D deformable body, as shown in Fig.S2. The analytical rigid body below was fully constrained through the reference points, where $U_1 = U_2 = U_3 = UR_1 = UR_2 = UR_3 = 0$.The analytical rigid body above was subjected to displacement boundary conditions, whereby $U_1 \neq 0$ or $U_2 \neq 0$. Additionally, all other degrees of freedom were set to 0, resulting in the body moving vertically downwards along either the X or Y direction. During the simulation, structural elements would come into contact. To account for this effect, general contact (Explicit) was selected to simulate. For the normal behavior, the "Hard" contact was selected and for the tangential behavior, the friction coefficient was set to 0.2.

4. Results and discussion

4.1. Deformation mechanisms and quasi-static compression characteristics

In this section, the deformation mechanism of the auxetic mechanics metamaterials was discussed and their quasi-static compression properties were characterized by a combination of numerical simulations. and experiments.

Fig. 2 displays the experimental curves of the auxetic metamaterials during quasi-static compression along the X and Y direction with the unit cell parameters: $L_1 = 12$ mm,$L_2 = 4$ mm,$d_1 = 2$ mm,$d_2 = 2$ mm,$t_1 = 0.6$ mm,$t_2 = 0.6$ mm,$s = 2.5$ mm. The curves can be classified into three regimes: the elastic regime, the plateau regime, and the densification regime. According to the compressed images and experimental curves, it is observed that the auxetic mechanical metamaterials possess negative Poisson's ratio behavior and energy absorption capability.

During compression, the specimens exhibit a negative Poisson's ratio behavior, and this effect is more obvious when compressed in the X direction than in the Y direction. During compression along the X direction, the inward-crossing inclined cell walls underwent bending deformation under the compressive load. As a result,d_1 became larger, causing the Y-direction cell walls of width t_1 to shrink inward. Consequently, the entire structure displayed a negative Poisson's ratio characteristic. The inward-crossing and outward-crossing inclined cell walls initially underwent bending deformation at the articulation point when compressed vertically. As the values of d_1 and d_2 increased, it was observed that the lateral length of the metamaterial shortened, exhibiting negative Poisson's ratio behavior. During the compression experiments, the upper and lower sections of the metamaterials were restricted by stiffening walls, causing a decrease in their inward contraction, and reducing the impact of the Poisson's ratio effect in compression with the middle segment of metamaterials.

During compression, metamaterials exhibited energy absorption ability. During compressed along the X direction, the initial stiffness was high, but the elastic stage was relatively short, entering the plateau stage rapidly. In the stress plateau stage, the dominant deformation mechanism was bending deformation, and the plateau stress remained stable. In the later stage of the plateau region, the structure exhibited weak stability leading to torsional deformation. Consequently, only the material at the center underwent plastic deformation, while the upper and lower parts connected to the stiffening walls experienced minor

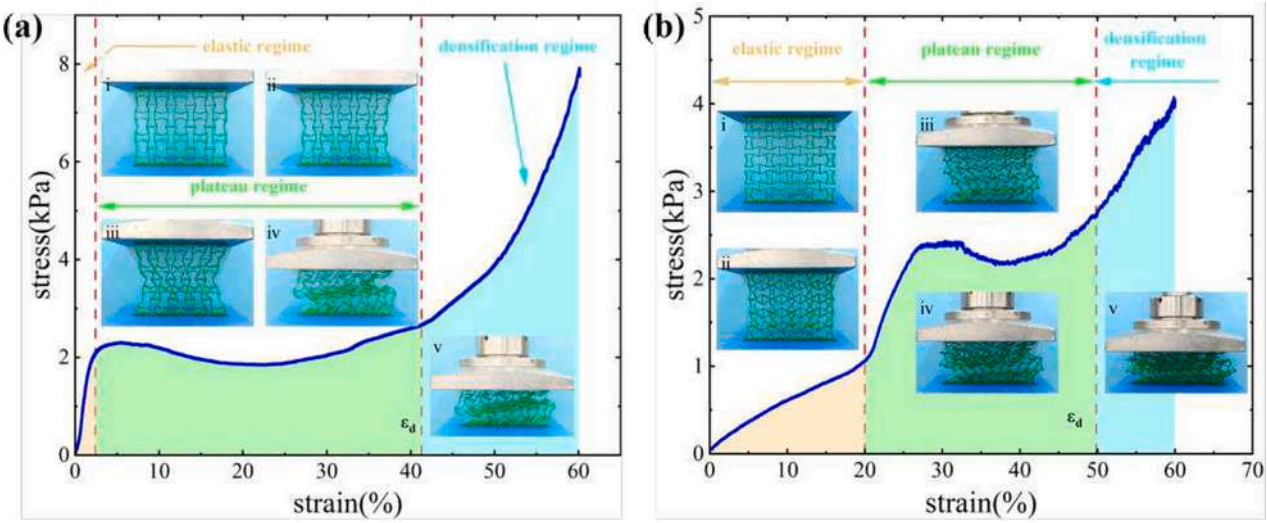

Fig. 2. The stress–strain curves of the metamaterials during compression along the (a) X direction and (b) Y direction

deformation, resulting in low material utilization rate [30]. When compressed along the Y direction, Y-direction cell walls of width t_1 moved down, causing the inclined cell walls to bend and rotate. The initial stiffness of the metamaterial was low, but the elasticity regime lasted for a long time. The elastic stage ended when the upper and lower surfaces of the X-direction cell walls of length $2L_2$ came into contact. Under compressive load, the inclined unit cell walls further bent, causing metamaterial to twist. This led to an increase in both the load-bearing capacity and elastic modulus. Subsequently, the specimen entered the plateau regime. Upon entering the densification regime, the structure became denser when compressed in various directions, subsequently causing a significant increase in load-bearing capacity.

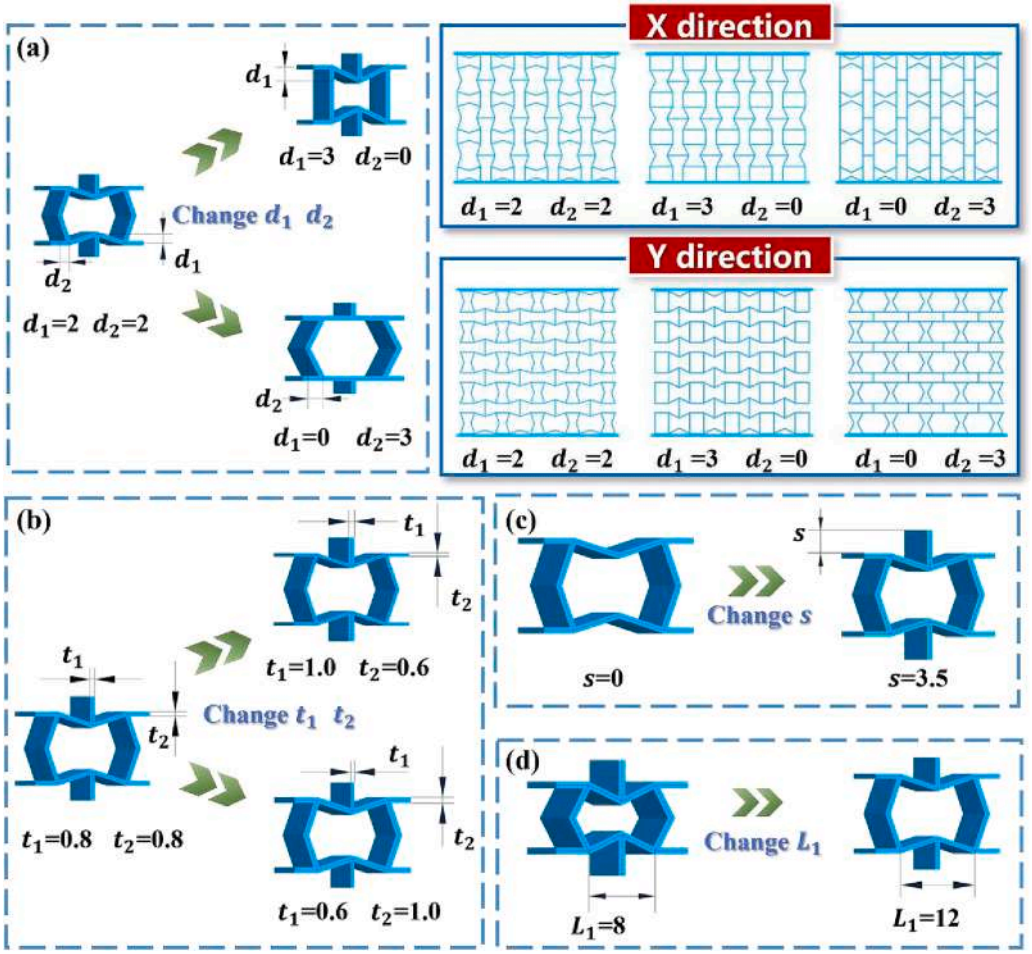

Fig. 3. Unit cell configuration with different geometric parameters: (a) different tilting distances d_1 and d_2; (b) different wall thicknesses t_1 and t_2; (c) different distances s; (d) different distances L_1.

4.2. Parameter analysis

The material distribution and characteristics of the auxetic mechanical metamaterials are influenced by the parameters of their structural geometry. Fig. 3(a) illustrates the unit cell configurations of inclined cell walls at different tilt distances and the CAD models of the specimen arrayed after. The variation ranges of d_1 and d_2 were from 0 mm to 3 mm, with an interval of 1 mm. The remaining parameters were set to: $L_1 = 12$ mm, $L_2 = 4$ mm, $t_1 = 0.6$ mm, $t_2 = 0.6$ mm, $s = 2.5$ mm.

The remaining parameters that have been studied included: cell wall thicknesses t_1,t_2 with a range of variation from 0.6 mm to 1.0 mm, the height s of the cell wall in the Y direction varies from 0 to 3.5 mm, the distance L_1 between the cell walls in the X direction varying from 8 mm to 12 mm. The cell configurations corresponding to the different geometrical parameters were displayed in Fig. 3(b)~(d).

4.2.1. Compression behavior

4.2.1.1. Along the X direction. First, to investigate the influence of d_1 and d_2 on the compression behavior of auxetic mechanical metamaterials along the X direction, Fig. 4 displays the experimental and simulation results when the parameters d_1 and d_2 are varied. As illustrated in Fig. 4(a), with $d_1 = 0$ and compression along the X direction, the inwardly inclined cell walls in the unit cell transformed into vertical walls along the X direction. The load-bearing capacity firstly increases rapidly during compression, and subsequently buckle after surpassing a threshold value. The middle segment of the material occurs bending deformation, and is extruded laterally, resulting in a rapid decrease in the load carrying capability. Thereafter, the plateau stress remains stable. And the deformation process is depicted in Fig. 5(a) and (b). In the compression process, there would be no negative Poisson's ratio. When d_1 is fixed at 0, the maximum load carrying capacity increases as d_2 increases. Simultaneously, the plateau stress is larger. When $d_1 = 1$ mm, the initial stiffness is basically the same under varying d_2. When d_2 changes from 0 to 2 mm, the plateau stress of the experimental curve increases gradually. The lowest value appears at $d_2 = 3$ mm.

As demonstrated in Fig. 4(b), a small peak appears on the stress–strain curve under compression because of the negative Poisson's ratio behavior within the metamaterial. When central material shrinks inward, it causes the X-direction cell walls of length $2L_2$ contacting with each other, and the structural stiffness increases, as shown in Fig. 5(c). When $d_1 = 2$ mm and $d_2 = 0$, the structure exhibits the highest load carrying capacity. Additionally, the stress value during the plateau stage

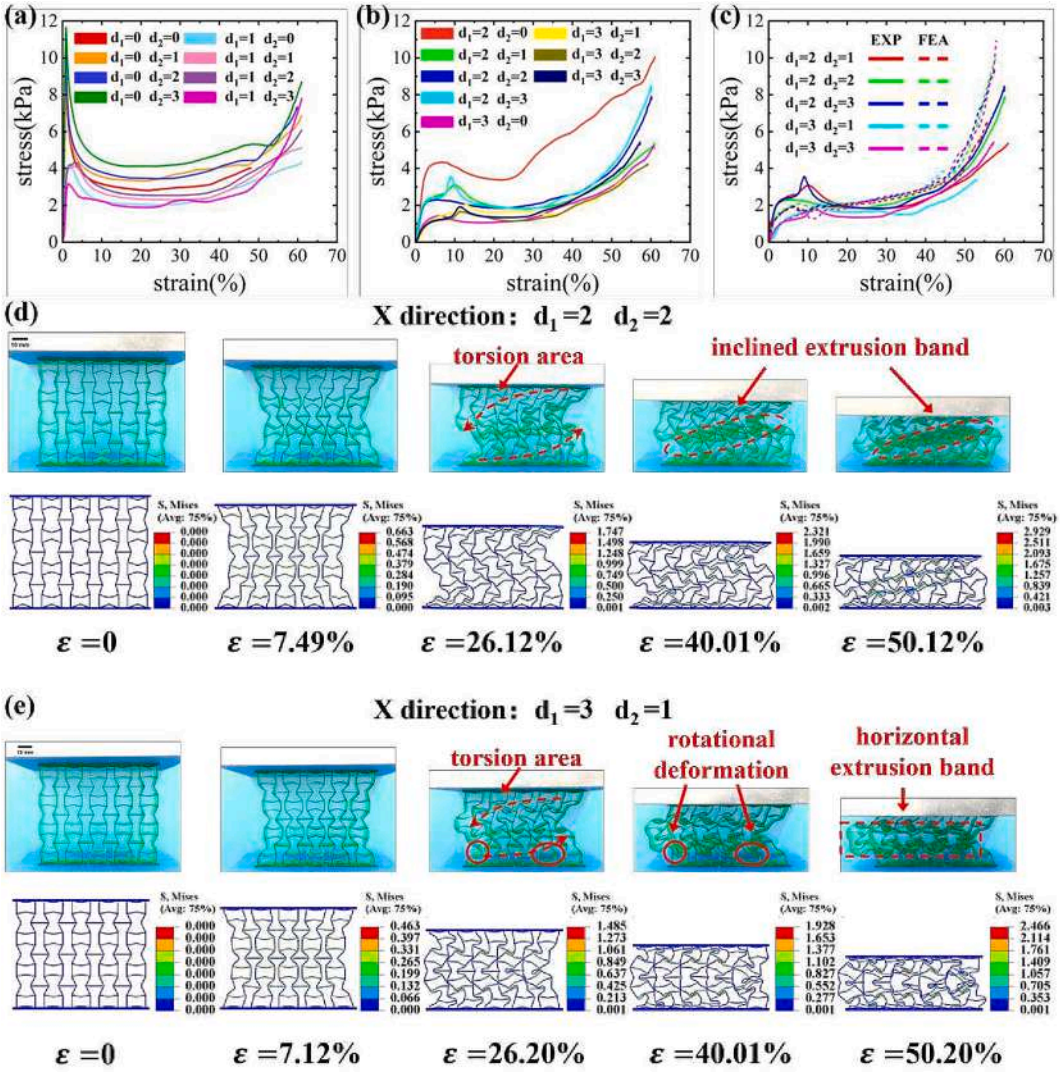

Fig. 4. Experimental compression curves along the X direction with (a) d_1=0 mm or d_1=1 mm and (b) d_1=2 mm or d_1=3 mm; (c) comparison of experimental and finite element curves for metamaterials compressed along the X direction; comparison of experiments and finite elements of compression deformation process with (d) d_1=2 mm, d_2=2 mm and (e) d_1=3 mm, d_2=1 mm.

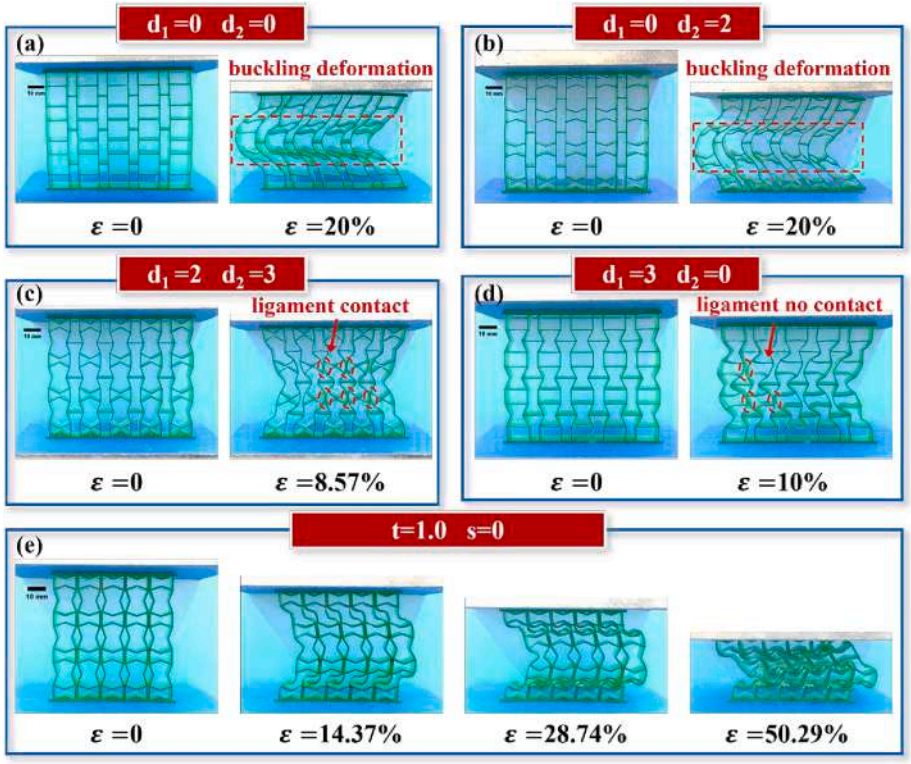

Fig. 5. The deformation maps of metamaterials compressed along the X direction under different unit cell parameters: (a) d_1=0 mm, d_2=0 mm; (b) d_1=0 mm, d_2=2 mm; (c) d_1=2 mm, d_2=3 mm; (d) d_1=3 mm, d_2=0 mm; (e) t=1.0 mm, s=0 mm

is greater than that observed under other parameters. This is because when $d_2 = 0$, the outward-crossing tilted cell walls in unit cell become horizontal cell walls along the Y direction. During the compression process, the force required for bending deformation exceeds that of the tilted cell walls. At $d_1 = 2$ mm, the plateau stress is almost the same as d_2 changes from 1 mm to 3 mm. During the process where $d_1 = 3$ mm and d_2 varies from 0 to 3 mm, the platform stress is almost the same. And when $d_1 = 3$ mm and $d_2 = 0$, the stress–strain curve is relatively smooth, this is because lateral bending occurs when the X direction cell walls do not contact each other, as shown in Fig. 5(d), and the structural stiffness has not been significantly strengthened. As compression displacement increases, the material undergoes further compaction, leading to a significant increase in load-bearing capacity.

Fig. 4(c)~(e) present metamaterials stress–strain curves compressed under certain parameters, as well as the experimental and finite element comparison of deformation process, which indicates high consistency. The possible reasons for the errors within the stress–strain curve include: the specimens were fabricated via light-curing printing, and there were manufacturing defects compared to the ideal finite element model; and after the preparation of the metamaterials, there would be a certain amount of residual strain, which caused an influence on the experimental results.

Observing the compression deformation process depicted in Fig. 4 (d), for the structure with parameters of $d_1 = 2$ mm and $d_2 = 2$ mm, the specimen first exhibits a negative Poisson's ratio behavior, leading to the material shrinking towards the center. Subsequently, as compression continues, the structural stability weakens, and torsional deformation occurs in the middle of the specimen while maintaining stable load-bearing capacity. The material in the middle undergoes rotation and enters the densification stage during the continued downward compression.

As depicted in Fig. 4(e), for the metamaterial with parameters of $d_1 = 3$ mm and $d_2 = 1$ mm, further compression is applied after the lateral contraction. Different from the specimen with unit cell parameters of $d_1 = 2$ mm and $d_2 = 2$ mm, the material located in the middle of the specimen firstly undergoes torsional deformation. Furthermore, with the increase in compression displacement, the central material moves towards the side of the specimen. Simultaneously, it drives the material linked to the upper and lower stiffening walls to generate a particular outward rotational deformation. Therefore, the material is extruded from the side, forming an extrusion band.

Second, the effect of cell walls thickness t_1 and t_2 on the auxetic metamaterials along the X direction was investigated. The ranges of variation for t_1 and t_2 were from 0.6 mm to 1 mm, with an interval of 0.2 mm. The other parameters remained unchanged, set as $L_1 = 12$ mm,$L_2 = 4$ mm,$d_1 = d_2 = 2$ mm,$s = 2.5$ mm. As demonstrated in Fig. 6 (a) and (b), compressive load-bearing capacity of the specimen along the X direction significantly improves with increasing t_2. Furthermore, the plateau stress rises from around 2 kPa to 9 kPa and 20–26 kPa. It is found that when the specimen produces a deformation pattern similar to that in Fig. 4(d), wherein an inclined extrusion band is generated in the middle of the specimen after undergoing torsional deformation, the plateau stress is determined to be high. When the specimen undergoes torsion in the middle and the material is extruded from the side, the material utilization rate is low, and the plateau stress is also low under this deformation mode. Observing Fig. 6(c), it is found that the experimental curves are basically consistent with those obtained by simulation. However, it is noteworthy that the elastic limit of finite element simulation curves are lower than that of the experimental curves, and this could be due to the following reason: the finite element simulation is an ideal case, where the deformation on both sides of the structures is uniform during compression, so the metamaterials enter the plateau stage relatively quickly. In contrast, auxetic metamaterials are not in ideal compression during the experiment, and there may exist an asynchrony in deforming the left and right sides, leading to a prolongation of the elastic stage. After entering the plateau region, the plateau stress of both is basically the same.

Third, the impact of L_1 on auxetic metamaterials along the X

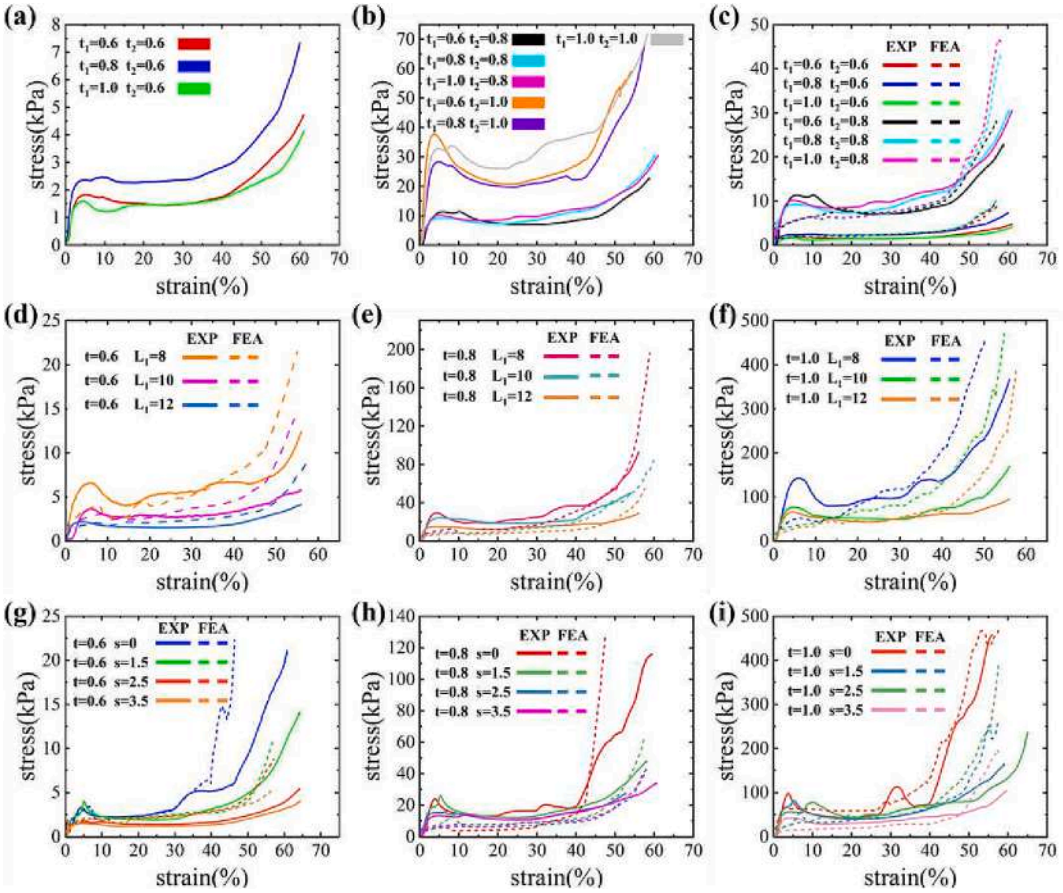

Fig. 6. Compression test curves along the X direction under the different geometric parameters and comparisons with finite elements: (a), (b) and (c): different wall thicknesses t_1, t_2; (d), (e) and (f): different distances L_1; (g), (h) and (i): different distances s.

direction was investigated. L_1 was set to $L_1 = 8$ mm, 10 mm, 12 mm in turn, while the remaining parameters were left unchanged. The setting is $L_2 = 4$ mm,$d_1 = d_2 = 2$ mm,$s = 2.5$ mm, and $t_1 = t_2$. As indicated in Fig. 6(d), (e), and (f), when the width t is constant, the metamaterials elastic limit gradually decreases progressively with increasing L_1 during compression, and the plateau stress also gradually decreases. This is because the deformation of the specimen mainly resulting from the bending of the inclined cell walls during compression. When the tilting distance of inclined cell wall remains constant, the larger L_1, the easier it is for the inclined cell wall to bend, and the smaller load required to be applied. Meanwhile, as the width t increases, the cell wall bending stiffness also increases, leading to a significantly enhancement in load-bearing capacity.

Finally, Fig. 6 (g), (h), and (i) represent the impact of s on the auxetic metamaterials along the X direction. The value of s was sequentially adjusted to $s = 0$, 1.5 mm, 2.5 mm and 3.5 mm, and the other parameters remained unchanged, with $L_1 = 12$ mm,$L_2 = 4$ mm,$d_1 = d_2 = 2$ mm,$t_1 = t_2$. As depicted in Fig. 6, when cell wall width t of metamaterial is fixed at a certain value, by observing the experimental images, the specimen plateau stress mainly depends on the deformation mode of the structure.

When $s = 0$, corresponding to canceling the arrangement of the Y-direction cell walls with width t_1, the X-direction cell walls with side length $2L_2$ were in contact with each other. During compression, apart from the top and bottom parts of the specimen with the height of $2L_2$, the material in the remaining area of the metamaterials is extruded from the side, and the deformation mainly results from the layer-by-layer buckling of the inward-crossing tilted cell walls. Fig. 5(e) shows that in this configuration, the metamaterials exhibit a higher load-bearing capacity, but no negative Poisson's ratio behavior is observed.

When unit cell parameters were set at $t = 0.6$ mm and $s = 1.5$ mm, the inclined cell walls are observed to bend upon compression, and the Y-direction cell walls shrink inward firstly. As compression continued, the Y-direction cell walls rotate, resulting in torsional deformation of the metamaterial. This forms an inclined extrusion band in the middle of the specimen with high plateau stress. When $t = 0.6$ mm,$s = 2.5$ mm and 3.5 mm, the metamaterial is compressed downward continuously after the contraction of the Y-direction cell walls. The Y-direction cell walls are extruded from the side while rotating, which leads to a poor material utilization and a low plateau stress. At $t = 0.8$ mm,$s = 1.5$ mm, 2.5 mm and 3.5 mm, the specimens all undergo torsional deformation, forming an inclined extrusion band in the middle of the specimen. Moreover, the plateau stress of all three are virtually identical. Similarly, when $t = 1.0$ mm,$s = 1.5$ mm, the metamaterial forms an inclined extrusion band during the compression process, resulting in a greater load carrying capability. However, when $s = 3.5$ mm, the material is extruded from the side and the plateau stress is lower.

In Fig. 6(d)-(i), there is a general trend whereby for large strain, the predicted stress by FEA is higher than that by experiment. One possible reason is that after sample preparation, there was slight damage, which expanded to a certain extent during compression, leading to a decrease in bearing capacity, while the damage was not considered in the finite element simulation.

4.2.1.2. Along the Y direction. First, Fig. 7 illustrates the stress–strain curves and finite element simulation results for varying the parameters d_1 and d_2, revealing their influence on the compression behavior of auxetic mechanical metamaterials along the Y direction. Fig. 7(a) illustrates the design drawing of specimen when compressed along the Y direction. Fig. 7(b) shows that all metamaterials, except for the one

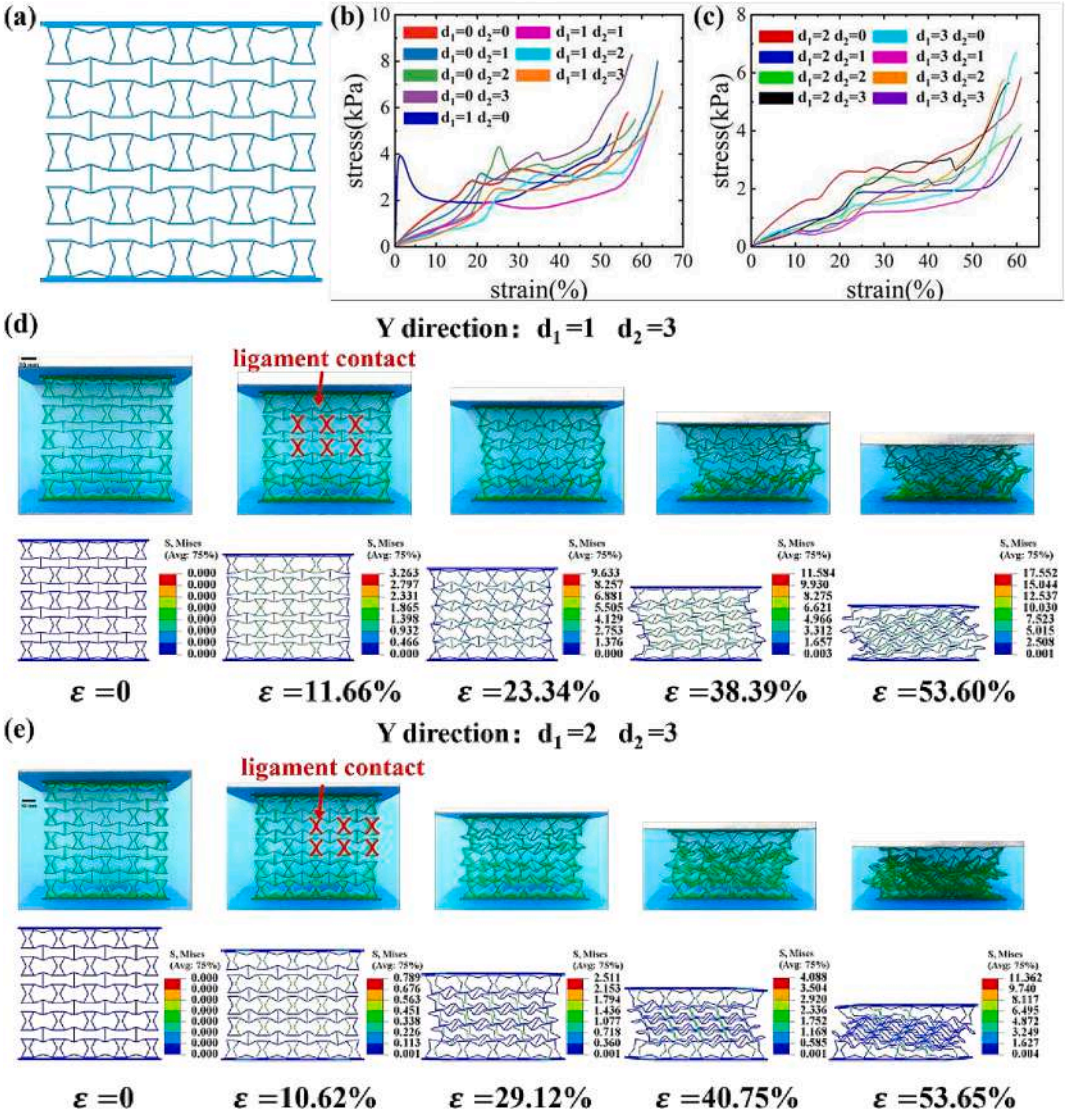

Fig. 7. (a) Design drawing of metamaterial compressed along the Y direction; experimental compression curves along the Y direction with (b) d_1=0 mm or d_1=1 mm (c) d_1=2 mm or d_1=3 mm; comparison of experiments and finite elements of compression deformation process with (d) d_1=1 mm, d_2=3 mm and (e) d_1=2 mm, d_2=3 mm.

corresponding to the unit cell parameters $d_1 = 1$ mm and $d_2 = 0$, have a longer elastic stage when compressed along the Y direction compared to compression along the X direction. The elastic strains can reach 17 % ~22 %. When d_1 is fixed, the initial stiffness of the specimen decreases as d_2 increase. When the unit cell parameters of metamaterial are $d_1 = d_2 = 0$, the structure tends to contract towards the center under the action of cell walls along the Y direction. However, the Y-direction cell walls are unstable during compression and are prone to tilting. The specimen bends under small strain, and the material is extruded from the center. Upon buckling, significant deformation and outward tilting occur first in the second and fourth layers, followed by the first and fifth layers, and finally the middles layer undergoes buckling, as illustrated in Fig. 8(a). When the metamaterial with parameters of $d_1 = 0, d_2 = 2$ mm is compressed for a certain distance, some of the cell walls along the X-direction with a length of $2L_2$ come into contact with each other, improving the load-bearing capacity of the metamaterial to some extent. Continuing compression causes the X-direction cell walls of neighboring cells to fully contact and compact, leading to a small peak in stress–-strain curve. Subsequently, the metamaterial collapses, leading to bending deformation. The load carrying capability decreases and stabilizes at a certain value, as depicted in Fig. 8(b). In the compression process, the Y-direction cell walls are unstable and prone to tilting and rotating. If the cell walls in the X-direction do not contact before the Y-direction cell walls tilt and rotate, the specimen stress–strain curve will be smooth.

It is also observed that when $d_1 = 0$ or 1 mm, the plateau stress is higher when $d_2 = 2$ mm and 3 mm, while it is lower at $d_2 = 0$ and 1 mm. This is because that with a larger initial value of d_2, the tilted cell walls that cross outwards are in contact with each other during compression, which improves the load-bearing capacity, as shown in Fig. 7(d) and (e), as well as Fig. 8(c).

Observing Fig. 7(c), when $d_1 = 2$ mm, the initial stiffness of the metamaterials drops as the increase of d_2. When $d_1 = 3$ mm, the initial stiffness of the metamaterial corresponding to $d_2 = 0$ is the highest, while the initial stiffness corresponding to $d_2 = 3$ mm is the lowest. The initial stiffness corresponding to $d_2 = 1$ mm and 2 mm is essentially identical, located between the first two.

When d_1 is fixed and d_2 varies from 1 mm to 3 mm, the plateau stress of the metamaterial is gradually increasing. This is because as d_2 increases, the outwardly inclined cell walls are more likely to contact with each other during compression, which enhances the load carrying capability. Observing the experimental curve of the metamaterial with

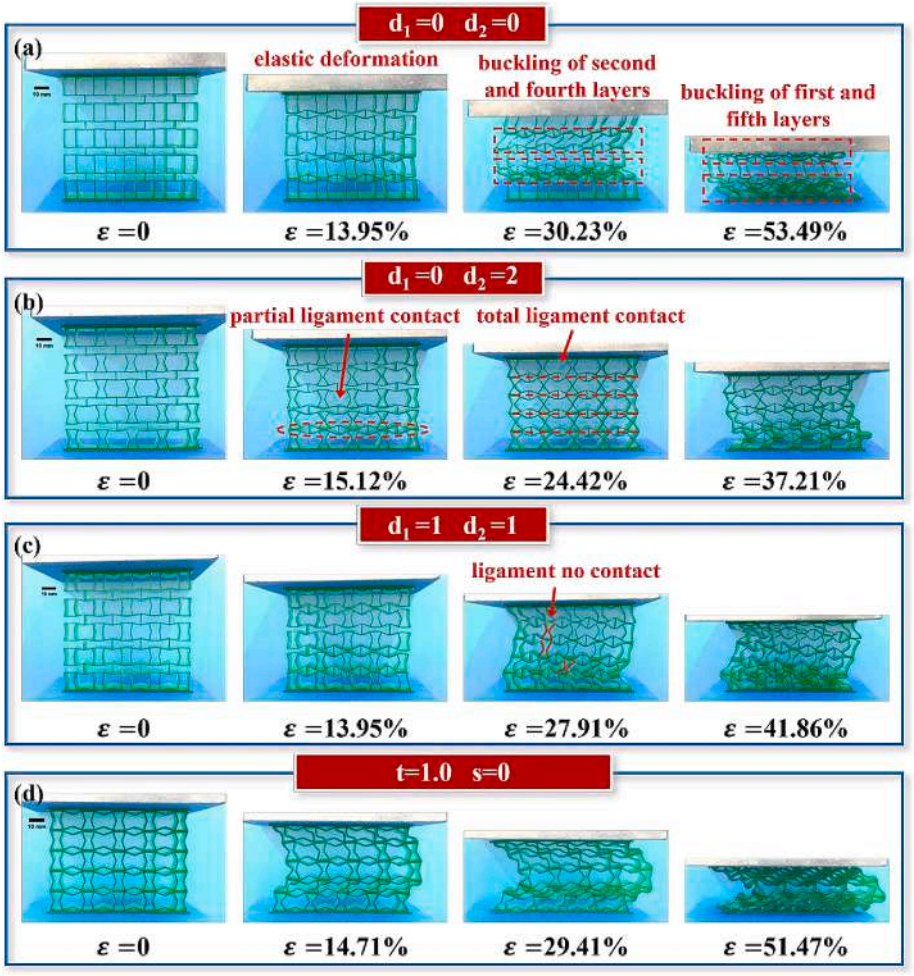

Fig. 8. The deformation maps of metamaterials compressed along the Y direction under different unit cell parameters: (a) d_1=0 mm, d_2=0 mm; (b) d_1=0 mm, d_2=2 mm; (c) d_1=1 mm, d_2=1 mm; (d) s=0 mm, t=1.0 mm.

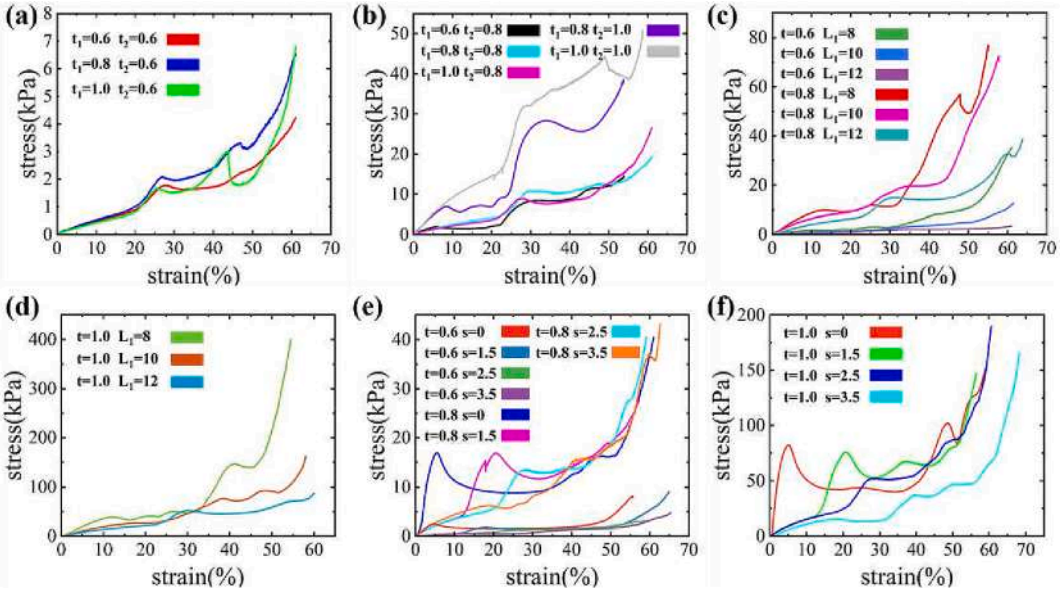

Fig. 9. Compression test curves along the Y direction of metamaterials under the different geometric parameters: (a) and (b): different wall thicknesses t_1, t_2; (c) and (d): different distances L_1; (e) and (f): different distances s.

unit cell parameters $d_1 = 2$ mm and $d_2 = 3$ mm, it is found that the load rapidly decreases at a strain of 46 %. This is caused by the collapse of the lowermost layer inclined cell walls during compression, which produces a certain degree of rotational deformation and rapidly reduces the bearing capacity.

Fig. 7(d) and (e) show the comparisons of experimental and simulation results of the compression deformation process under certain parameters. The results demonstrate high consistency between the two. During compression, the Y-direction cell walls move downwards, causing the inclined cell walls to first undergo bending deformation, with d_1 and d_2 increasing. The metamaterials contract inward, exhibiting negative Poisson's ratio effect. During compression, the Y-direction cell walls may tilt and rotate, causing buckling and the disappearance of the negative Poisson's ratio behavior. As the compression continues, the inclined cell walls further bend and deform, leading to denser structures and forming a compression band in the middle of the metamaterials, which enhances their load-baring capacity.

Second, the effect of cell walls thickness t_1 and t_2 on auxetic metamaterials along the Y direction was investigated, and the parameter settings were the same as Fig. 6. From Fig. 9(a) and (b), the initial stiffness and the plateau stress of metamaterials increase significantly with the increase of t_2. Observing the experimental images, when $t_1 \geqslant t_2$, the metamaterials exhibit greater stability during compression, and the Y-direction cell walls with width t_1 are less prone to buckle. The metamaterials possess a higher stiffness and load-bearing capacity. When $t_1 < t_2$, the Y-direction cell walls are prone to buckling and rotating during compression, resulting in lower stiffness and reduced load carrying capability of metamaterials. Observing Fig. 9(a), the compression curve of the metamaterial with unit cell parameters of $t_1 = 1.0$ mm, $t_2 = 0.6$ mm exhibits a significant oscillation. This is due to the rapid gliding between the outward-crossing tilted cells in the middle layer after contact, leading to a sudden reduction in load carrying capacity.

Third, the impact of L_1 on auxetic metamaterials along the Y direction was carried out with the same parameter settings as in Fig. 6. From Fig. 9 (c) and (d), when the metamaterials are compressed along the Y direction, the initial stiffness decreases gradually with an increase in L_1, for a given cell walls width t. Additionally, the plateau stress also gradually decreases. Similar to compression along the X direction, the deformation of metamaterial is primarily induced by bending the inclined cell walls. When the inclined distance remains constant, the larger L_1, the easier it is for the inclined cell walls to bend, and the smaller load required to be applied. Meanwhile, as the width t grows, the bending stiffness of cell walls also rises, and thus metamaterials load bearing capacity is also significantly enhanced.

Finally, Fig. 9(e) and (f) represent the effect of cell walls height s on the auxetic metamaterials along the Y direction, and the parameter settings were the same as Fig. 6. When $s = 0$, the X-direction cell walls with length $2L_2$ were touching each other. During compression, the outward-crossing tilted cell walls bend and drive the X-direction cell walls with length of $2L_2$ to move laterally, causing the metamaterials to undergo buckling deformation. Under this parameter, the initial stiffness is at its maximum, but the load-bearing capacity is not, meanwhile, there is no negative Poisson's ratio effect, as illustrated in Fig. 8(d).

When the cell walls width t is constant and the value of s varies from 1.5 mm to 3.5 mm, the initial stiffness of the metamaterials is basically the same. However, the strain entering the plateau stage raises with the increase of s. The main deformation during the elastic stage is the downward displacement of the Y direction cell walls, and their contraction towards the middle. When the cell walls of width $2L_2$ contact with each other, the load-bearing capacity of the specimen increases significantly. When $s = 3.5$ mm, the Y-direction cell walls with width t_1 are unstable, and they are prone to tilting and rotating under compressive load, resulting in the extrusion of material from the side. The metamaterials load carrying capability increases markedly when horizontal call walls of the upper and lower cells are in contact. The performance of metamaterials remains the same with respect to the effect of cell wall width t: the larger t is, the higher load carrying capability of the metamaterials is.

4.2.2. Negative Poisson's ratio

In this article, the mechanical metamaterials proposed exhibit negative Poisson's ratio behavior. This is because the bending of inclined cell walls during compressed along the X or Y direction. The experimental process was not an ideal vertical compression as there were manufacturing defects in the prepared specimens. Additionally, the finite element simulated deformation process closely resembled the experimental deformation process. Therefore, the displacement of marked points from finite element model was chosen to characterize the negative Poisson's ratio. The supporting information lists the selection of model marker points and the process for calculating Poisson's ratio.

4.2.2.1. Along the X direction. Fig. 10 illustrates how the Poisson's ratio changes with strain when the metamaterials are compressed along the X direction. As compression strain rises, the absolute value of Poisson's ratio falls.

Observing Fig. 10(a), as the unit cell parameter d_1 increases, the contraction behavior of the inward-crossing tilted cells becomes weaker, leading to the absolute value of Poisson's ratio decreasing. When d_1 is certain, the larger of d_2 is, the larger the absolute Poisson's ratio. This is because when d_1 is certain, an increase in d_2 weakens the bending stiffness of the outward-crossing inclined cell walls. Therefore, it is easier to produce larger bending deformation in compression, causing the metamaterials to contact inwardly and enhancing the negative Poisson's ratio behavior.

Fig. 10(b) shows that, in general, the parameters t_1 and t_2 have little effect on the Poisson's ratio. When $t_2 = 1.0$ mm,$t_1 = 0.6$ mm or 1.0 mm, the negative Poisson's ratio changes by 43 % from -2.81 to -1.59 as the strain increase from 1 % to 5 %. For all other unit cell parameters, the Poisson's ratio changes slowly, from around -2.67 to around -1.86, a change of about 30 %.

Observing Fig. 10(c), when the metamaterials are compressed along the X direction, the bending stiffness of inclined cell walls decreases as the unit cell parameter L_1 increase, which leads to a reduction in initial stiffness of metamaterials. The reduction of structural stiffness means an increase in structural deformation capacity [30], so the transverse contraction is more obvious, and the negative Poisson's ratio behavior is enhanced. When L_1 is constant, the absolute Poisson's ratio also grows as the cell wall thickness t increases.

When considering parameter s, the absolute Poisson's ratio decreases with increasing s. The reason for this is that an increase in s result in an increase in the length of the metamaterials along the Y direction, causing a decrease in strain along the Y direction at the same shrinkage distance. When the longitudinal strain of the metamaterials remains constant along the X direction, the negative Poisson's ratio property weakens. Meanwhile, the absolute value of negative Poisson's ratio increases with the increase in the thickness t of the cell walls.

4.2.2.2. Along the Y direction. Fig. 11 displays the correlation of Poisson's ratio and strain for metamaterials with varying geometrical parameters when compressed along the Y direction. Overall, the absolute value of Poisson's ratio increases as compression strain rises.

Observing Fig. 11(a), the absolute Poisson's ratio of metamaterials increases as the unit cell parameter d_1 increases. This is because the initial stiffness of the specimens decreases, resulting in an improvement in the deformation ability and enhancement of the negative Poisson's ratio behavior. As d_2 increases, the absolute value of Poisson's ratio decreases when d_1 is certain.

Considering parameters t_1 and t_2, as shown in Fig. 11(b), when t_2 is certain, the Poisson's ratio hardly changes despite changes t_1. When t_1 is constant, the absolute Poisson's ratio is the highest at $t_2 = 0.6$ mm, and the Poisson's ratio remains similar at $t_2 = 0.8$ mm and 1.0 mm. In the

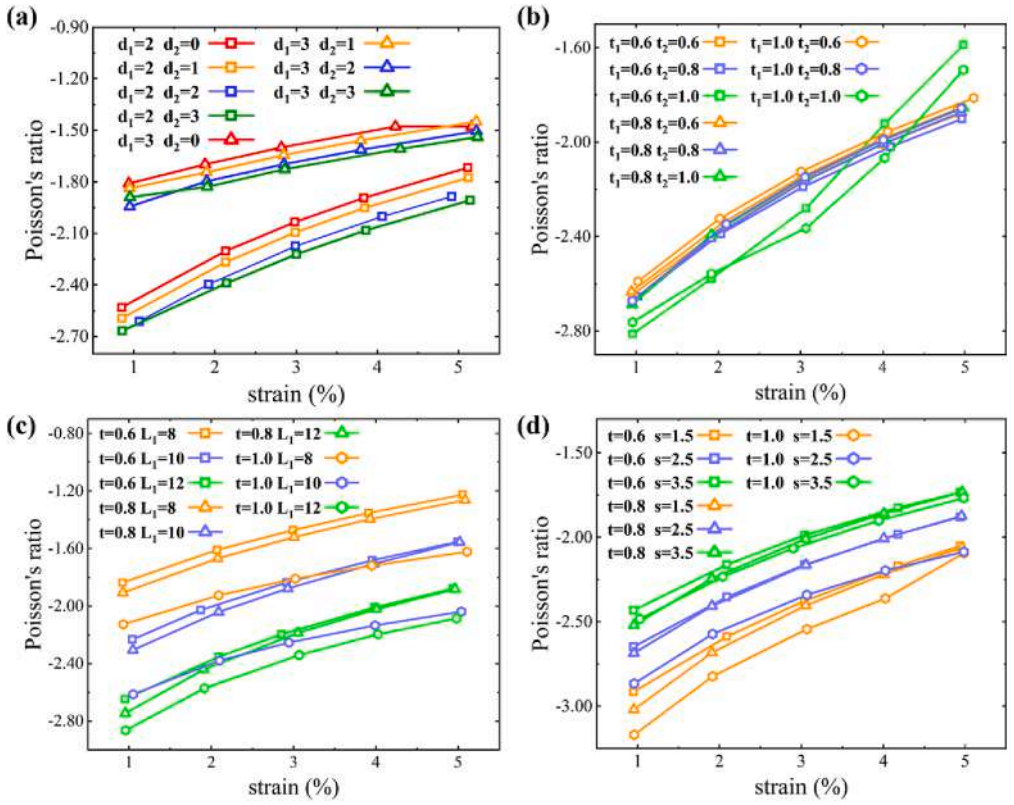

Fig. 10. Variation of Poisson's ratio with strain in compression along the X direction for metamaterials with different geometrical parameters:(a) different tilting distances d_1, d_2; (b) different wall thicknesses t_1, t_2; (c) different distances L_1; (d) different distances s.

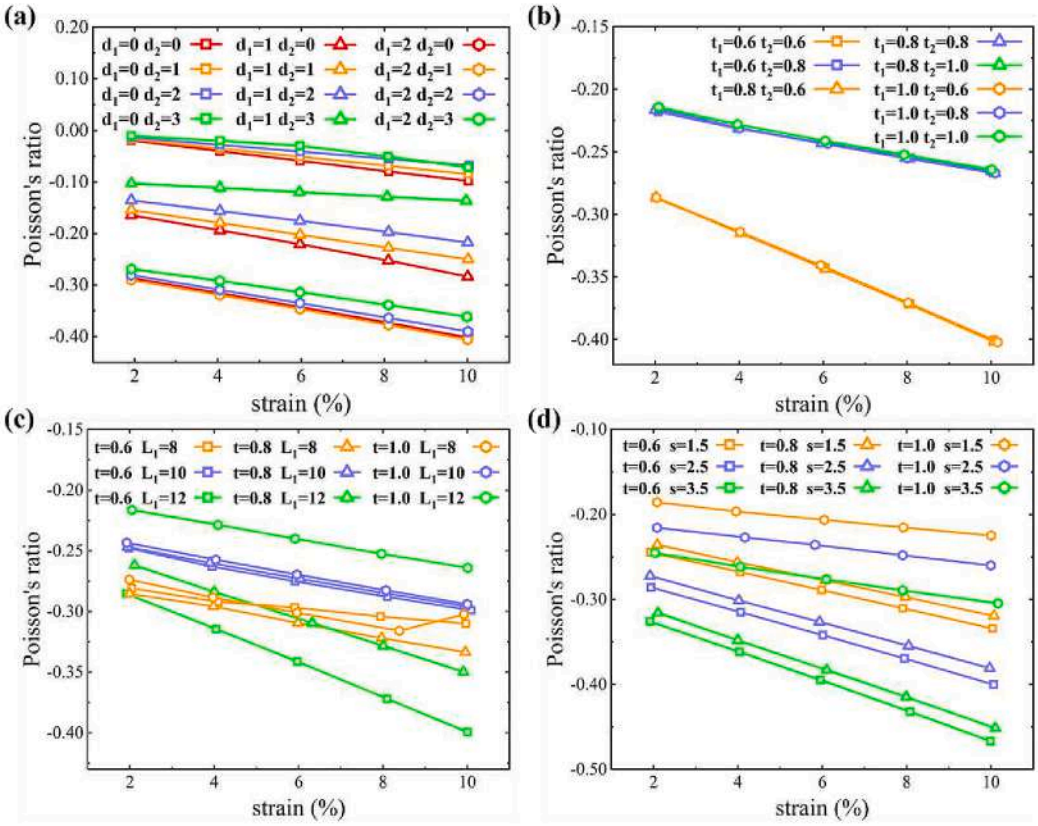

Fig. 11. Variation of Poisson's ratio with strain in compression along the Y direction for metamaterials with different geometrical parameters:(a) different tilting distances d_1, d_2; (b) different wall thicknesses t_1, t_2; (c) different distances L_1; (d) different distances s.

strain range of 2 % to 10 %, the absolute Poisson's ratio at $t_2 = 0.8$ mm and 1.0 mm decreases by approximately 25 % to 34 % compared to $t_2 = 0.6$ mm.

Observing Fig. 11(c), when the metamaterials are compressed along the Y direction, the Poisson's ratio hardly changes with variation in the thickness t at $L_1 = 8$ mm and 10 mm. When $L_1 = 12$ mm, the absolute Poisson's ratio gradually decreases as the thickness of cell walls t increase. The absolute values of negative Poisson's ratio gradually decrease as the cell walls thickness t remains constant and L_1 changes from 8 mm to 10 mm.

When $t = 1$ mm and $L_1 = 8$ mm, the absolute value of Poisson's ratio suddenly decreases at a strain of 10 %. This is because the stiffness of the Y-direction cell walls under this parameter is poorer than that of the inclined cell walls. When compressed to a certain extent, the Y-direction cell walls first buckle, causing the inclined cell walls in the third row to extrude outward, and the lateral contraction effect disappears. From a parameter perspective, when L_1 is fixed at 8 mm and the length of the Y-direction cell walls is constant, the stiffness of the Y-direction cell walls and the inclined cell walls are increasing with the increase of the cell wall thickness t. However, the increase in the stiffness of the inclined cell walls is more significant. On the other hand, when the cell wall thickness t is fixed, the stiffness of the inclined cell walls increases as L_1 decreases. Therefore, under the parameters of $t = 1$ mm and $L_1 = 8$ mm, the specimen buckles at 10 % strain.

Considering parameter s, the absolute values of Poisson's ratio raise as the increase of s when the cell walls thickness t is certain. This is because the increase of s means the enhance of the longitudinal height of the metamaterials. Therefore, the longitudinal strain declines under the same compression displacement, causing the absolute values of negative Poisson's ratio to increase.

When s is fixed and t is varied from 0.6 mm to 0.8 mm, the absolute Poisson's ratio decreases to a certain extent, and when it is varied to 1.0 mm, the Poisson's ratio is significantly weakened.

4.2.3. Energy absorption characteristics

To assess the energy absorption capability, researchers have proposed some evaluation indicators, such as total energy absorption (EA), specific energy absorption (SEA), densification strain ε_d and energy absorption efficiency η. The SEA refers to the capacity of energy absorption per unit mass, and the densification strain is the maximum strain value of the structure before being compacted.

The equations for calculating EA and SEA when compressing specimen along X direction are as follows:

$$EA = \int_0^{\delta_{xd}} F(\delta_x) d\delta_x \tag{1}$$

$$SEA = \frac{EA}{m} \tag{2}$$

where δ_x and δ_{xd} are the displacement and the densification deformation in the X direction, $F(\delta_x)$ is the compressive load, and m is the metamaterial mass.

The energy absorption efficiency η and the densification strain ε_d are obtained from the following two equations:

$$\eta(\varepsilon_x) = \frac{\int_0^{\varepsilon_x} \sigma(\varepsilon_x) d\varepsilon_x}{\sigma(\varepsilon_x)} \tag{3}$$

$$\left.\frac{d\eta(\varepsilon_x)}{d\varepsilon_x}\right|_{\varepsilon_x=\varepsilon_d} = 0 \tag{4}$$

where $\sigma(\varepsilon_x)$ and ε_x are the nominal stress and the nominal strain along X direction during compression.

Fig. 12 displays the EA and SEA of metamaterials with varying unit cell parameters when compressed along the X direction, and the parameters corresponding to each model are also enumerated in the figure. When compressed along the X direction, at $d_2 = 0$, metamaterials exhibit a gradual increase in energy absorption as d_1 varies from 0 to 2 mm, with the weakest energy absorption occurring at $d_1 = 3$ mm. When d_2 varies from 1 mm to 3 mm, both the EA and SEA gradually decline as d_1 increase. Compared with $d_1 = d_2 = 0$ (which is a positive Poisson's ratio honeycomb), when the tilted cell walls of the specimen are tilted at a non-zero distance, the maximum increase in EA and SEA can be up to 133 % and 123 %. When the unit cell parameter t_1 remains constant, the EA of the metamaterials improves significantly as t_2 increases. Overall, parameter t_1 has little impact on the EA, and during $t_1 = t_2 = 1$ mm, the EA and SEA of the specimen are the maximum. Observing Fig. 12, the cell wall thickness t has a greater impact on the EA of metamaterials compared to L_1 and s. Furthermore, EA is markedly improved by increasing the cell wall thickness. More details about the energy absorption along the X direction were presented in Fig. S4 in the supporting information.

Fig. 13 shows the EA and SEA with varying unit cell parameters when compressed along the Y direction, and the parameters corresponding to each model are also enumerated in the figure. In general, when d_2 is certain, the plateau stress declines with the increase of d_1, and both EA

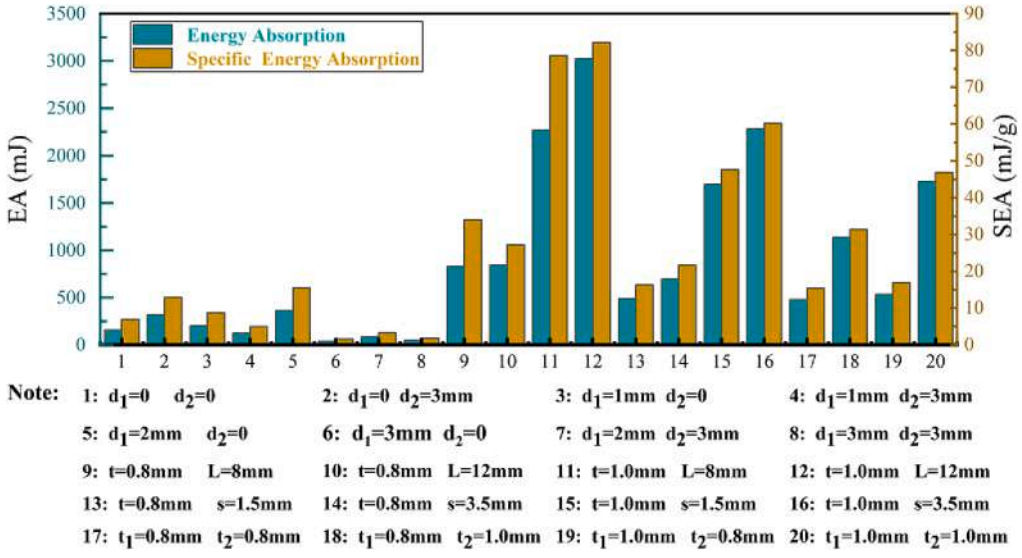

Fig. 12. EA and SEA in compression along the X direction for specimens with different unit cell geometrical parameters.

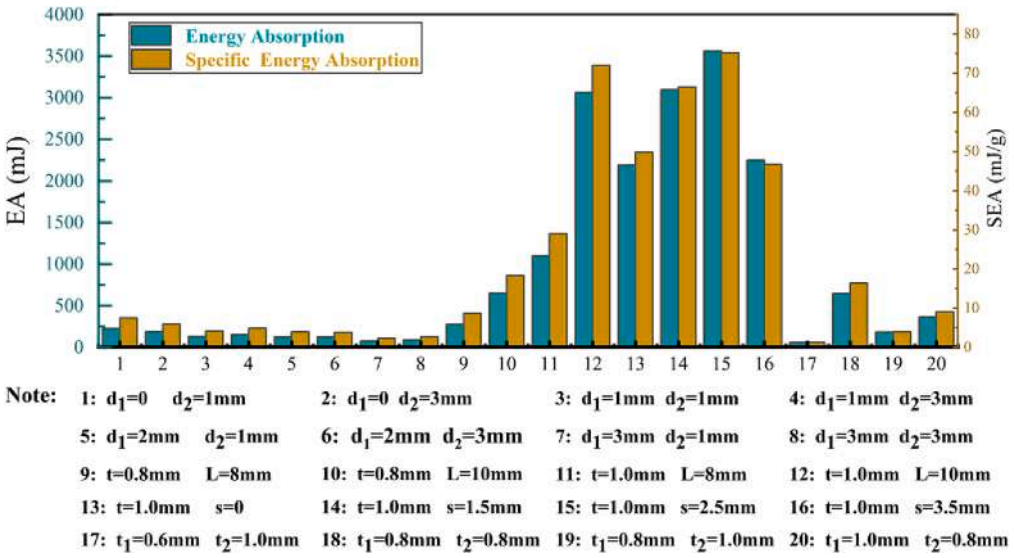

Fig. 13. EA and SEA in compression along the Y direction for specimens with different unit cell geometrical parameters.

and SEA decrease gradually. Compared with $d_1 = d_2 = 0$, when the tilted cell walls of the specimen are tilted at a non-zero distance, the maximum increase in EA and SEA can be up to 11 % and 6 %. When t_1 and t_2 are close to each other, the specimens are more stable and exhibit greater energy absorption capacity, such as $t_1 = t_2 = 0.6$ mm, $t_1 = t_2 = 0.8$ mm and $t_1 = t_2 = 1.0$ mm. Metamaterials are prone to buckling during compression, leading to a drop in energy absorption capacity when there is a significant difference between t_1 and t_2, such as $t_1 = 0.6$ mm, $t_2 = 1.0$ mm and $t_1 = 1.0$ mm, $t_2 = 0.6$ mm, etc. The results indicated that the EA of metamaterials can be enhanced by both the unit cell parameters t and L_1. Although the initial stiffness and the plateau stress decrease as L_1 increases, the densification strain increases, resulting in the enhancement of the EA. The load carrying capability of the metamaterials and the EA are significantly enhanced as the width t of cell walls increases. As depicted in Fig. 13, when s is small, the elastic stage of metamaterials is prolonged with the increase of s. However, the plateau stress after stabilization remains basically the same. Therefore, the EA enhances with the raise of s. However, as the value of s increase, the Y-direction cell walls are more prone to buckling and rotating during compression, leading to material extrusion from the sides. In this case, metamaterials exhibit lower load-bearing and energy absorption capacities. And further details about the energy absorption along the Y direction were presented in Fig. S5 in the supporting information.

4.3. Characterization of reconfigurable properties

The technology used for preparing mechanical metamaterials was LCD light curing 4D printing technology, and the resin used was shape memory photosensitive resin, so the manufactured metamaterials possessed shape memory effect. Shape programming and shape reconfigurable experiments were conducted in a hot water bath, and compressive testing were conducted on the programmed metamaterials.

The specific programming and reconstruction process was as follows: firstly, the manufactured metamaterial was placed in hot water and subjected to a vertical tensile or compression displacement along the Y direction to program it into a temporary configuration. The specimen was then cooled to room temperature while maintaining the external force, and the external force was released to make it maintain in the temporary configuration, as shown in the middle pictures of Fig. 14(b) and Fig. 14(c). The tensile strain was 5.75 % in the pre-tension state and the compressive strain was 9.20 % in the pre-compression state. Finally, the metamaterials were returned to their initial state under thermal excitation by placing them in hot water again. The restored configurations are shown in the images on the right side of Fig. 14(b) and Fig. 14(c).

Fig. 14(a) displays the nominal stress–strain curves generated from the compression experiments performed on the specimens in the initial configuration, pre-tension configuration and pre-compression

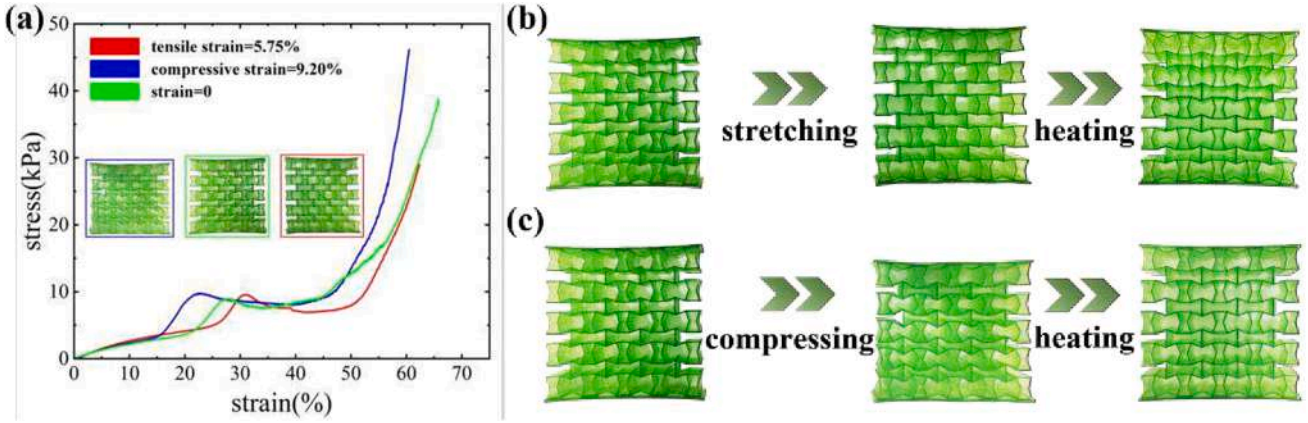

Fig. 14. Characterization of the programmable and reconfigurable properties of the metamaterials: (a) stress–strain curves of the metamaterials in different configurations; (b) the stretching and heating recovery process; (c) the compressing and heating recovery process.

configurations. The stress plateau of the specimen under pre-compression configuration appears earlier, while the stress plateau of the specimen under pre-tension configuration appears later. Thus, the programmable and reconfigurable 4D printed auxetic mechanics metamaterials are realized by means of a hot water bath.

5. Conclusions

This work proposes an auxetic mechanics metamaterial that utilizes 4D printing technology and shape memory material to achieve negative Poisson's ratio and energy absorption capability. Firstly, deformation mechanisms and in-plane compressive mechanical characteristics are investigated by quasi-static compression tests and numerical simulations. The results indicate that the dominant deformation mechanism during in-plane compression is bending deformation, which avoids stress oscillation during the deformation process and can be applied as an energy absorber. When compressed along the X direction, two deformation modes are exhibited, forming inclined or horizontal extrusion bands. When compressed along the Y direction, a horizontal compression band is generated. Secondly, the effect of the geometrical parameters on both energy absorption and Poisson's ratio are analyzed. The metamaterials demonstrate negative Poisson's ratio behavior along both X and Y directions. When compressed along the X direction, the energy absorption capability improves significantly with an increase of t_2. When compressing in the Y direction, if t_1 and t_2 are close to each other, they exhibit a larger energy absorption capacity. Finally, the programmable and reconfigurable demonstration of mechanical metamaterials is accomplished by means of hot water bath, providing a method for the post-fabrication modification of the mechanical characteristics of metamaterials.

CRediT authorship contribution statement

Bingxun Li: Writing – review & editing, Writing – original draft, Methodology, Investigation, Conceptualization. **Xiaozhou Xin:** Visualization, Investigation, Formal analysis, Conceptualization. **Cheng Lin:** Visualization, Methodology, Formal analysis. **Liwu Liu:** Writing – review & editing, Supervision, Methodology, Investigation, Conceptualization. **Yanju Liu:** Writing – review & editing, Supervision. **Jinsong Leng:** Writing – review & editing, Supervision.

Declaration of competing interest

The authors declare that they have no known competing financial interests or personal relationships that could have appeared to influence the work reported in this paper.

Data availability

Data will be made available on request.

Acknowledgements

The authors gratefully acknowledge the financial support provided by the National Key R&D Program of China (2022YFB3805700), the National Natural Science Foundation of China (Grant Nos. 12072094 and 12172106) and Self-Planned Task (NO.SL20230101) of Songjiang Laboratory, Harbin Institute of Technology

Appendix A. Supplementary data

Supplementary data to this article can be found online at https://doi.org/10.1016/j.compstruct.2024.118135.

References

[1] Yu X, Zhou J, Liang H, Jiang Z, Wu L. Mechanical metamaterials associated with stiffness, rigidity and compressibility: a brief review. Prog Mater Sci 2018;94:114–73.
[2] Kildishev AV, Boltasseva A, Shalaev VM. Planar photonics with metasurfaces. Science 2013;339:1232009.
[3] Schittny R, Kadic M, Guenneau S, Wegener M. Experiments on transformation thermodynamics: molding the flow of heat. Phys Rev Lett 2013;110:195901.
[4] Guo X, Ni X, Li J, Zhang H, Zhang F, Yu H, et al. Designing mechanical metamaterials with kirigami-inspired, hierarchical constructions for giant positive and negative thermal expansion. Adv Mater 2020;33:2004919.
[5] Tan X, Li Y, Wang L, Yao K, Ji Q, Wang B, et al. Bioinspired flexible and programmable negative stiffness mechanical metamaterials. Advanced Intelligent Systems 2023;5:2200400.
[6] Meza LR, Das S, Greer JR. Strong, lightweight, and recoverable three-dimensional ceramic nanolattices. Science 2014;345:1322–6.
[7] Bauer J, Schroer A, Schwaiger R, Kraft O. Approaching theoretical strength in glassy carbon nanolattices. Nature Mater 2016;15:438–44.
[8] Yin Y, Yu Y, Li B, Chen G. Notch flexure as kirigami cut for tunable mechanical stretchability towards metamaterial application. Int J Smart Nano Mater 2022;13:203–17.
[9] Zhang Q, Dong J, Zhao Y, Zheng Y. Three-dimensional meta-architecture with programmable mechanical properties. Int J Smart Nano Mater 2022;13:152–65.
[10] Lim T-C. Mechanics of Metamaterials with Negative Parameters. Singapore: Springer Nature; 2020.
[11] Lim T-C. Auxetic Materials and Structures. Singapore: Springer Science+Business Media; 2015.
[12] Liu K, Han L, Hu W, Ji L, Zhu S, Wan Z, et al. 4D printed zero Poisson's ratio metamaterial with switching function of mechanical and vibration isolation performance. Mater Des 2020;196:109153.
[13] Zhang L, Pan F, Ma Y, Yang K, Guo S, Chen Y. Bistable reconfigurable origami metamaterials with high load-bearing and low state-switching forces. Extreme Mech Lett 2023;63:102064.
[14] Frenzel T, Kadic M, Wegener M. Three-dimensional mechanical metamaterials with a twist. Science 2017;358:1072–4.
[15] Fernandez-Corbaton I, Rockstuhl C, Ziemke P, Gumbsch P, Albiez A, Schwaiger R, et al. New twists of 3D chiral metamaterials. Adv Mater 2019;31:1807742.
[16] Zeng Q, Duan S, Zhao Z, Wang P, Lei H. Inverse design of energy-absorbing metamaterials by topology optimization. Adv Sci 2022;10:2204977.
[17] Zhang X, Wang J, Sun Q, Li J, Zhou S, Qi J, et al. Mechanical design and analysis of bio-inspired reentrant negative Poisson's ratio metamaterials with rigid-flexible distinction. Int J Smart Nano Mater 2023:2246928.
[18] Zhang P, Qi D, Xue R, Liu K, Wu W, Li Y. Mechanical design and energy absorption performances of rational gradient lattice metamaterials. Compos Struct 2021;277:114606.
[19] Lakes R. Foam structures with a negative poisson's ratio. Science 1987;235:1038–40.
[20] Lim T-C. A partially auxetic metamaterial inspired by the maltese cross. United Kingdom: Cambridge University Press; 2022.
[21] Lakes R. Composites and Metamaterials. Singapore: World Scientific; 2020.
[22] Hu H, Zhang M, Liu Y. Auxetic Textiles. United Kingdom: Woodhead Publishing; 2019.
[23] Huang Z, Hao Y, Li Y, Hu H, Wang C, Nomoto A, et al. Three-dimensional integrated stretchable electronics. Nat Electron 2018;1:473–80.
[24] Wu Z, Zhao J, Wu W, Wang P, Wang B, Li G, et al. Radial compressive property and the proof-of-concept study for realizing self-expansion of 3D printing polylactic acid vascular stents with negative poisson's ratio structure. Materials 2018;11:1357.
[25] Meeusen L, Candidori S, Micoli LL, Guidi G, Stankovi T, Graziosi S. Auxetic structures used in kinesiology tapes can improve form-fitting and personalization. Sci Rep 2022;12:13509.
[26] Pan Q, Chen S, Chen F, Zhu X. Programmable soft bending actuators with auxetic metamaterials. Sci China Technol Sci 2020;63:2518–26.
[27] Lazarus A, Reis PM. Soft actuation of structured cylinders through auxetic behavior. Adv Eng Mater 2015;17:815–20.
[28] Li X, Peng W, Wu W, Xiong J, Lu Y. Auxetic mechanical metamaterials: from soft to stiff. Int J Extrem Manuf 2023;5:042003.
[29] Han D, Ren X, Zhang Y, Zhang X, Zhang X, Luo C, et al. Lightweight auxetic metamaterials: design and characteristic study. Compos Struct 2022;293:115706.
[30] Li K, Zhang Y, Hou Y, Su L, Zeng G, Xu X. Mechanical properties of re-entrant anti-chiral auxetic metamaterial under the in-plane compression. Thin-Walled Struct 2023;184:110465.
[31] Wang S, Liu H-T. Enhancement design and quasi-static crushing response of novel star-rhombus honeycombs. Physica Status Solidi (b) 2023:2300231.
[32] Farzaneh A, Pawar N, Portela CM, Hopkins JB. Sequential metamaterials with alternating Poisson's ratios. Nat Commun 2022;13:1041.
[33] Wu X, Su Y, Shi J. In-plane impact resistance enhancement with a graded cell-wall angle design for auxetic metamaterials. Compos Struct 2020;247:112451.
[34] Liu H, Zhang ET, Ng BF. In-plane dynamic crushing of a novel honeycomb with functionally graded fractal self-similarity. Compos Struct 2021;270:114106.
[35] Jackson JA, Messner MC, Dudukovic NA, Smith WL, Bekker L, Moran B, et al. Field responsive mechanical metamaterials. Sci Adv 2018;4:eaau6419.
[36] Dudek KK, Martínez JAI, Ulliac G, Hirsinger L, Wang L, Laude V, et al. Micro-scale mechanical metamaterial with a controllable transition in the poisson's ratio and band gap formation. Adv Mater 2023;35:2210993.

[37] Wagner M, Chen T, Shea K. Large shape transforming 4D auxetic structures. 3D Print Addit Manuf 2017;4:133–41.
[38] Lei M, Hong W, Zhao Z, Hamel C, Chen M, Lu H, et al. 3D printing of auxetic metamaterials with digitally reprogrammable shape. ACS Appl Mater Interfaces 2019;11:22768–76.
[39] Xin X, Liu L, Liu Y, Leng J. 4D printing auxetic metamaterials with tunable, programmable, and reconfigurable mechanical properties. Adv Funct Mater 2020; 30:2004226.